Computing the Probability of Local Brain Connectivity using Diffusion Tensor Imaging

Joshua S. Shimony[1], Adrian A. Epstein[1], and G. Larry Bretthorst[2]

Mallinckrodt Institute of Radiology[1] and Department of Chemistry[2],
Washington University Medical School
521 S. Kingshighway Blvd., St. Louis, MO 63110, USA

Abstract. The diffusion tensor model has been used to analyze magnetic resonance diffusion data and has been successful in both neuroscientific and clinical applications. We propose an enhancement of this model with a local connectivity parameter that better accords with the known structure of white-matter. In addition to providing diffusion tensor parameter estimation the calculation provides the probability that a given pixel is connected to one of its nearest neighbors. These probabilities can be used in further calculations to determine the probability of connectivity between different brain regions. Implementation of the algorithm is discussed in addition to its usage in simulated and in-vivo magnetic resonance diffusion tensor data.

Keywords: Diffusion Tensor Imaging, DTI, MRI, Brain Connectivity
PACS: 02.50.Cw

INTRODUCTION

Diffusion, the random thermal motion of microscopic particles, has been of great scientific interest ever since its initial description in 1827 by Robert Brown (hence the term "Brownian motion"). He observed this motion while using a microscope to examine a collection of pollen particles floating in a water droplet. Stejskal and Tanner [1] first proposed a method to measure diffusion in liquid samples early in the development of nuclear magnetic resonance spectroscopy and this was later applied to magnetic resonance (MR) imaging by Le Bihan *et al.* [2, 3]. The clinical use of diffusion imaging expanded rapidly after its sensitivity to the early detection of stroke was demonstrated [4-7].

When diffusion occurs in an isotropic medium, it is uniform in all directions and well described by a single diffusion parameter. Visually, this can be understood as the spherical diffusive spread of a small drop of dye in a uniform media. In biological tissue, diffusion displacements are hindered unevenly in three-dimensional (3D) space by cell membranes and other sub-cellular constituents. This uneven diffusion can be quantified and is termed diffusion anisotropy. It is especially prominent in tissue with a regular structural organization, such as nerve or muscle fibers. Visually, the diffusive spread of a drop of dye in this medium will form a 3D ellipsoidal shape. The dye will spread a greater distance along the direction of the nerve fibers, but will be relatively restricted in the direction perpendicular to them [8-11].

The use of the diffusion tensor (DT) model to describe the anisotropic 3D diffusive spread of water in the brain as measured with MR was first proposed by Basser *et al.* [12]. This model relies on a symmetric 3x3 diffusion matrix which represents the size of the diffusion coefficient in different directions in space as a 3D ellipsoid. In practice seven parameters are estimated for each image pixel from numerous MR diffusion measurements, each sensitized to diffusion to a different degree and in a different direction. In MR imaging the sensitization to diffusion is achieved by turning on a pair of pulsed magnetic field gradients. The first gradient pulse tags the proton spins by causing them to precess rapidly and increase the phase shifts across the image. The second gradient pulse is turned on in the opposite direction to the first and unwinds the phase shifts caused by the first pulse. Any proton that diffuses away from its original position during the interval between the gradient pulses will not completely re-phase and will cause signal loss in the image. The amount of signal loss in the diffusion image as compared to the original image gives an estimate of the diffusion in the direction of the pulsed gradients.

The estimated parameters can be understood as three diffusion coefficients along the axes of the ellipsoid (diffusion eigenvalues) and three angles that represent the direction of the ellipsoid in space. In equation form, the signal S is a function of a gradient vector $\mathbf{q} = \gamma\mathbf{G}\delta$ ($\mathbf{G}$ the gradient vector, γ the gyromagnetic ratio for protons, δ the gradient width) and can be expressed as

$$S(\mathbf{q}) = S(0)\exp\left\{-\Delta\mathbf{q}\mathbf{D}\mathbf{q}^T\right\} + C \qquad (1)$$

in which $S(0)$ is the baseline signal with gradients turned off, Δ is the inter-gradient delay, and $\mathbf{D}$ is a symmetric 3x3 diffusion matrix. The diffusion matrix can be specified in term of its eigenvalues, λ_1, λ_2, λ_3, and three rotation angles, φ, θ, ψ, as seen in the relationship

$$\mathbf{D} = \mathbf{R}(\varphi,\theta,\psi)\begin{pmatrix}\lambda_1 & 0 & 0\\ 0 & \lambda_2 & 0\\ 0 & 0 & \lambda_3\end{pmatrix}\mathbf{R}^T(\varphi,\theta,\psi) \qquad (2)$$

where $\mathbf{R}$ is a 3x3 rotation matrix. The constant C represents a component of the signal that arises from highly constrained water molecules, and has been found to improve the representation of the data [13, 14]. Estimation of $S(0)$, C, the three rotation angles, and the three eigenvalues provides for eight adjustable parameters in this model. Standard analysis of data using the DTI formalism makes the assumption that each pixel is an independent diffusion compartment and that the diffusion follows the Gaussian model, *i.e.* the solution of the diffusion equation represents the probability of a water molecule diffusing as a Gaussian function of the displacement distance.

Brain connectivity, defined as the anatomical and functional (white-matter) connections between the computational units (gray-matter) of the brain is of great interest to neuroscientists and physicians. In the past connectivity information was limited and only available from human pathological specimens and from invasive studies, usually in non-human primates. Given the sensitivity of DT imaging to the local direction of nerve fiber bundles it has the potential to provide information on brain connectivity in a non-invasive manner. Many approaches have been used to derive connectivity information from DT data [15-17] and some have made good use of Bayesian probability theory to estimate the model parameters [15]; however most

of these attempts have solved each pixel independently of its neighbors. In this project we extend the standard DT model by including a local connectivity parameter, Λ, and then use Bayesian probability theory to compute the probability that a given pixel is connected to its neighbors. Although introducing this connectivity parameter complicates the parameter estimation, this provides a more accurate model of the structure of the brain since it is known that nerve fiber bundles can extend across long distances in the brain, well over the dimension of a single imaging pixel. By adding the connectivity parameter we include in the model our prior anatomic information of the structure of the brain, information that is ignored by models that treat each pixel independently.

METHODS

Bayesian Inference and Markov chain Monte Carlo

Unlike the simple case of estimating the DT parameters for each pixel separately, the addition of the connectivity parameter creates a global problem of estimation where each pixel depends on the parameters of its neighbors. Each pixel has nine parameters to be determined, six (3 eigenvalues and 3 angles) from the diffusion tensor (**D, in bold**), the baseline signal of the measurement, $S(0)$, the additive constant C, and the connectivity parameter, Λ. We express the DT parameters for pixel i as Ω_i:

$$\Omega_i = \{\lambda_{1i}, \lambda_{2i}, \lambda_{3i}, \varphi_i, \theta_i, \psi_i, S_i(0), C_i, \Lambda_{ij}\}, \quad (3)$$

where Λ_{ij} is the connectivity parameter for pixel i, and j specifies its 26 nearest neighbors (the neighbors to a pixel are contained in a 3x3x3 cube surrounding it). The total parameter space (Ω) includes the entire N pixels in the image:

$$\Omega = \{\Omega_1, \Omega_2, \Omega_3, \ldots, \Omega_N\} \quad (4)$$

The probability for the DT parameters given the data (*D, italicized,* not to be confused with the diffusion tensor, **D**, represented in bold), and relevant background information I is expressed in terms of Bayes' theorem [18] as

$$P(\Omega|DI) \propto P(D|\Omega I)P(\Omega|I) \quad (5)$$

where $P(D|\Omega I)$ is the direct probability for the data given the model parameters, and $P(\Omega|I)$ is the prior probability for the model parameters. We factor this expression:

$$P(\Omega|DI) = \prod_{i=1}^{N} P(D_i|\Omega_i I)P(\Omega_i|I). \quad (6)$$

The prior probability for the parameters in a given pixel, $P(\Omega_i|I)$, can be factored using the product rule and logical independence into a series of eight prior probabilities:

$$P(\Omega_i|I) \propto P(\lambda_{1i}|I)P(\lambda_{2i}|I)P(\lambda_{3i}|I)P(\varphi_i|I)P(\theta_i|I)\ldots P(\Lambda_{ij}|I). \quad (7)$$

The rotation angles were assigned uniform prior probabilities. The remaining parameters (with the exception of the connectivity parameter) were assigned Gaussian prior probabilities bounded by an appropriate physiologic range.

The connectivity parameter does not appear in the DT model, consequently in this calculation it appears only in the prior probabilities. The preference for connectivity is

indicated by the prior probability of Λ_{ij}, which we expressed as the probability that a water molecule will diffuse from the central pixel to a neighboring pixel along a line connecting the two. According to the DT model the probability for a water molecule to travel a distance **r**, can be represented as a Gaussian function. An accurate calculation would require a path integral but we approximate the probability of diffusion across adjacent pixels as the product of two Gaussian distributions, one from the *i*th pixel, representing the first half of the motion of the water molecule, and the second from the neighboring pixel, representing the second half. If $\mathbf{r}_{ij}$ expresses the distance between the two pixels, Δ is the inter-gradient delay, and $\mathbf{D}_i$ and $\mathbf{D}_j$ the diffusion tensors of the two pixels, the prior probability can be patterned after the real probability as:

$$P(\Lambda_{ij}|I) \propto \exp\left\{-\frac{w\Delta}{\mathbf{r}_{ij}\mathbf{D}_i\mathbf{r}_{ij}^T}\right\}\exp\left\{-\frac{w\Delta}{\mathbf{r}_{ij}\mathbf{D}_j\mathbf{r}_{ij}^T}\right\}, \tag{8}$$

with *w* being an adjustable weighting factor.

The direct probability for the data, given the DTI measurements in a given pixel, $P(D_i|\Omega_i I)$, is a marginal probability when the standard deviation, σ_i, was removed using the sum and product rules:

$$P(D_i|\Omega_i I) = \int P(\sigma_i D_i|\Omega_i I)d\sigma_i \propto \int P(\sigma_i|I)P(D_i|\sigma_i\Omega_i I)d\sigma_i. \tag{9}$$

Although the standard deviation of the noise is fairly uniform in the central portion of the image it has a strong dependence on position toward the periphery. Consequently, we assume a different σ_i for each pixel in the image. Assigning a Jeffreys' prior probability for $P(\sigma_i|I)$ and assigning the direct probability for the data, $P(D_i|\sigma_i\Omega_i I)$, using a Gaussian, the marginal probability for the data, $P(D_i|\Omega_i I)$, may be written as:

$$P(D_i|\Omega_i I) = \frac{1}{2}\Gamma\left(\frac{M}{2}\right)\left(\frac{Q}{2}\right)^{-M/2} \tag{10}$$

resulting in the Student's *t*-distribution, where *M* is the number of data points per pixel and Q_i is the total square residual given by:

$$Q_i = \sum_{k=1}^{M}\left(E_{ik} - S_i(\mathbf{q}_k)\right)^2 \tag{11}$$

with E_i being the experimental diffusion measurements.

Substituting Eq. [7] and Eq. [10] into Eq. [6] results in an expression for the posterior probability for all of the parameters with only the prior $P(\Lambda_{ij}|I)$ linking each pixel *i* to its neighbors. The joint posterior probability for all of the parameters was sampled using a Metropolis-Hastings Markov chain Monte Carlo simulation with simulated annealing [19, 20].

Introducing the connectivity parameter complicates the parameter estimation because each pixel is dependent, via the connectivity prior, on the parameter values of its neighbors. When performing the calculations on a parallel processor it is important to insure that the neighboring pixels do not change while the estimation of the *i*th pixel is underway. We implemented this calculation by an iterative scheme that is analogous in 1-dimension to doing all the even pixels first and then returning to do the odd pixels. In 3D this requires 8 separate passes through the data to cover all the pixels in the sample once.

Simulated and Experimental Data

The algorithm was tested using a small simulated data set that was 3x3x3 pixels in size. This provided us with a single pixel and its 26 immediate nearest neighbors. The initial data values in the 27 pixels were set to simple examples with known answers to test the algorithm under different circumstances. From the known preset values of the parameters we generated the results that would be measured in a typical MR experiment with the addition of Gaussian noise.

The algorithm was then applied to a single slice of DT measurements performed on a 1.5T Siemens Sonata scanner (Erlangen, Germany) in a normal volunteer. In addition to anatomic T1- and T2-weighted images the DT data was acquired using a locally modified echo planar imaging sequence in 37 directions with 3 separate gradients strengths (b-value = 400-1200s/mm^2, TE = 113ms, TR = 7s). All data processing was done using a locally written software package.

RESULTS

Figure 1A represents the probability distribution for the connectivity parameter in a simulated experiment with a single fiber passing through the sample volume. All the neighboring pixels in these cases have the same anisotropy and are pointing in the same direction as the central pixel. The highest connectivity is seen with the two neighboring pixels that are pointed to by the fiber direction (coded as directions 10 and 16 in this case). The change in the connectivity parameter with a change in anisotropy (=0.15, 0.30, and 0.7) is demonstrated in the figure, giving the expected increase in the probability along the preferred directions with increased anisotropy. These values of anisotropy were selected to represent the typical range of anisotropy values in the brain, from dense white matter (0.7) to just above gray matter (0.15).

Figure 1B represents the probability distribution for the connectivity parameter in a simulated experiment with two crossing fibers passing through the sample volume. Resolving crossing fibers represents one of the major challenges with current methods for estimating brain connectivity. In this case the highest connectivity is seen with four neighboring pixels (coded as directions 10, 12, 14, and 16), two for each one of the fiber directions. The change in the connectivity parameter is also demonstrated with a change in the anisotropy, again demonstrating the expected increase in the connection probability along the preferred directions with an increase in anisotropy.

Figure 2 presents the results from applying the model to a data set acquired from the brain of a healthy volunteer. The image on the left is an anisotropy image of a coronal section, approximately in the middle of the brain. The bright regions in the image are of areas of white matter with high anisotropy, and the darker regions are of gray matter with low anisotropy. The marked white square on the left has been magnified and is displayed on the right of the image. Superposed on the magnified view are red whiskers that give an indication of the value of the connectivity parameter in each pixel. A larger connectivity is indicated by a longer whisker. The full results, which are in 3D, are limited by the 2D representation in the image, and

demonstrate a strong resemblance to the known anatomy in this area. Region 1 in this figure is of a patch of gray matter with low anisotropy, which is indicated by several approximately equal whiskers pointing in different directions without a dominant nerve fiber bundle. Region 2 represents the corpus callosum which is one of the

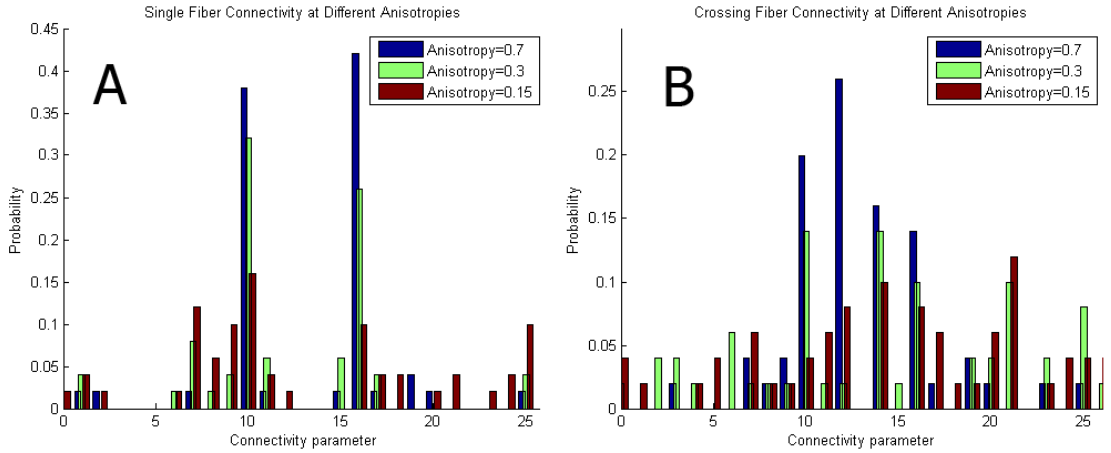

FIGURE 1. (A) The probability distribution of the connectivity parameter for the case of a single fiber. The preferred connectivity to two neighboring pixels is demonstrated in addition to changes in the distribution with a change in anisotropy. See text for further details. (B) The probability distribution of the connectivity parameter for the case of two crossing fibers. The preferred connectivity to four neighboring pixels is demonstrated in addition to changes in the distribution with a change in anisotropy. See text for further details.

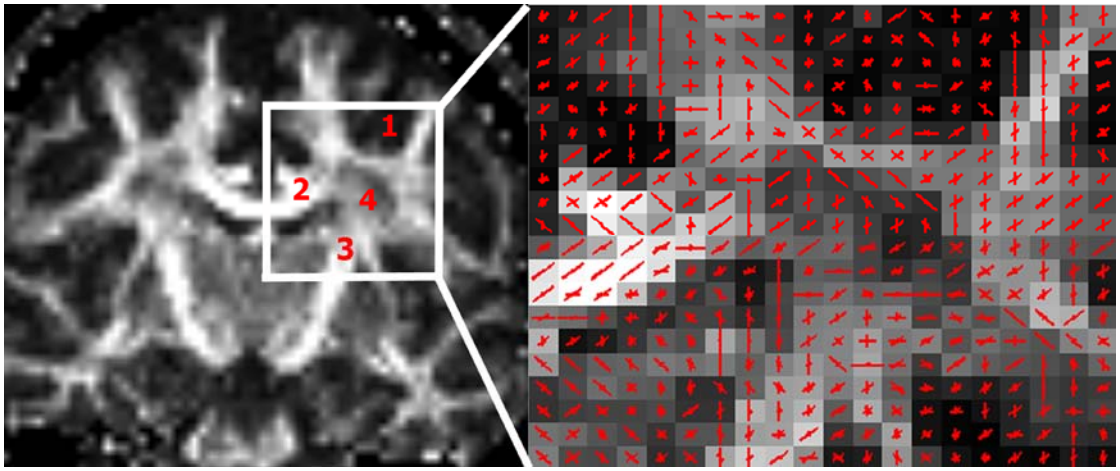

FIGURE 2. The connectivity parameter in a data set from the brain of a normal subject. The image on the left is an anisotropy image of a coronal section of the brain. The image on the right is a magnification of the region marked by the white square with superposed red whiskers indicating the value of the connectivity parameter in each pixel. See text for further details.

largest and most anisotropic fiber bundles in the brain. The whiskers in this region are very uniform and point in the dominant medio-lateral direction. Region 3 represents the internal capsule, which is also a dense fiber bundle that extends in the superior-

inferior direction and is well represented by the whiskers. Region 4 contains many crossing fibers, which are represented in the whisker plot as small crosses.

SUMMARY

We have implemented an enhanced model for estimation of the DT from MR data of the brain using local connectivity information that better accords with the known structure of white-matter. Standard DT models treat each pixel separately and do not account for the fact that nerve fiber bundles in white matter of the brain can extend over many pixels and relatively large distances in the brain. In addition to providing diffusion tensor parameter estimation the calculation provides the probability that a given pixel is connected to one of its nearest neighbors. These probabilities can be used in further calculations to determine the probability of connectivity between different brain regions, a result that is of great research and clinical interest. We demonstrated preliminary results of this algorithm in both a small simulated data set with known expected results, and in a real diffusion data set obtained in the brain of a healthy volunteer, in which it demonstrated results that are in accord with the known anatomy. Future work will use the local connectivity results to calculate the probability that various regions in the brain are connected.

ACKNOWLEDGMENTS

We would like to thank NIH K23 HD053212 and National Multiple Sclerosis Society PP1262 for generous financial support.

REFERENCES

1. Stejskal, E.O. and J.E. Tanner, *Spin diffusion measurements: Spin echoes in the presence of time-dependent field gradients.* J. Chem. Phys., 1965. **42**: p. 288-292.
2. LeBihan, D., et al., *MR imaging of intravoxel incoherent motions: Application to diffusion and perfusion in neurologic disorders.* Radiology, 1986. **161**: p. 401-407.
3. LeBihan, D., et al., *Separation of diffusion and perfusion in intravoxel incoherent motion MR imaging.* Radiology, 1988. **168**: p. 497-505.
4. Moseley, M.E., et al., *Early detection of regional cerebral ischemia in cats: Comparison of diffusion- and T_2-weighted MRI and spectroscopy.* Magn. Reson. Med., 1990. **14**: p. 330-346.
5. Le Bihan, D., et al., *Diffusion MR imaging: clinical applications.* AJR Am J Roentgenol, 1992. **159**(3): p. 591-9.
6. Chien, D., et al., *MR diffusion imaging of cerebral infarction in humans.* AJNR Am J Neuroradiol, 1992. **13**(4): p. 1097-102; discussion 1103-5.
7. Warach, S., et al., *Fast magnetic resonance diffusion-weighted imaging of acute human stroke.* Neurology, 1992. **42**: p. 1717-1723.
8. Moseley, M.E., et al., *Diffusion-weighted MR imaging of anisotropic water diffusion in cat central nervous system.* Radiology, 1990. **176**: p. 439-445.
9. Hajnal, J.V., et al., *MR imaging of anisotropically restricted diffusion of water in the nervous system: technical, anatomic, and pathologic considerations.* J Comput Assist Tomogr, 1991. **15**(1): p. 1-18.
10. Chenevert, T.L., J.A. Brunberg, and J.G. Pipe, *Anisotropic diffusion in human white matter: demonstration with MR techniques in vivo.* Radiology, 1990. **177**: p. 401-405.

11. Beaulieu, C. and P.S. Allen, *Determinants of anisotropic water diffusion in nerves.* Magn. Reson. Med., 1994. **31**: p. 394-400.
12. Basser, P.J., J. Mattiello, and D. LeBihan, *MR diffusion tensor spectroscopy and imaging.* Biophys. J., 1994. **66**: p. 259-267.
13. Bretthorst, G.L., C.D. Kroenke, and J.J. Neil. *Characterizing water diffusion in fixed baboon brain*. in *24th International workshop on Bayesian inference and maximum entropy methods in science and engineering*. 2004. Garching, Germany.
14. Kroenke, C.D., et al., *Diffusion MR imaging characteristics of the developing primate brain.* Neuroimage, 2005. **25**(4): p. 1205-13.
15. Behrens, T.E.J., et al., *Characterization and propagation of uncertainty in diffusion-weighted MR imaging.* Magn Reson Med, 2003. **50**: p. 1077-1088.
16. Mangin, J., et al., *A framework based on spin glass models for the inference of anatomical connectivity from diffusion-weighted MR data - a technical review.* NMR Biomed, 2002. **15**: p. 481-492.
17. Parker, G.J.M., H.A. Haroon, and C.A.M. Wheeler-Kingshott, *A framework for a streamline-based probabilistic index of connectivity (PICO) using a structural interpretation of MRI diffusion measurements.* J Magn Reson Imaging, 2003. **18**: p. 242-254.
18. Jaynes, E.T., *Probability Theory: the logic of science*, ed. G.L. Bretthorst. 2003, Cambridge: Cambridge University Press.
19. Gilks, W.R., S. Richardson, and D.J. Spiegelhalter, *Markov Chain Monte Carlo in Practice*. 1996, London: Chapman and Hall.
20. Metropolis, N., et al., *Equation of state calculation by fast computing machines.* J Chem Phys, 1953. **21**: p. 1087-1092.